A TWO-STAGE 100 L/min CIRCUMFERENTIAL SLOT VIRTUAL IMPACTOR SYSTEM FOR BIOAEROSOL CONCENTRATION

A Thesis

by

DANIEL EDWARD LACROIX

Submitted to the Office of Graduate Studies of
Texas A&M University
in partial fulfillment of the requirements for the degree of

MASTER OF SCIENCE

August 2008

Major Subject: Mechanical Engineering

A TWO-STAGE 100 L/min CIRCUMFERENTIAL SLOT VIRTUAL IMPACTOR SYSTEM FOR BIOAEROSOL CONCENTRATION

A Thesis

by

DANIEL EDWARD LACROIX

Submitted to the Office of Graduate Studies of
Texas A&M University
in partial fulfillment of the requirements for the degree of

MASTER OF SCIENCE

Approved by:

Chair of Committee,	Andrew McFarland
Committee Members,	Yassin Hassan
	Bryan Shaw
Head of Department,	Dennis L. O'Neal

August 2008

Major Subject: Mechanical Engineering

ABSTRACT

A Two-Stage 100 L/min Slot Virtual Impactor System for Bioaerosol Concentration.
(August 2008)
Daniel Edward LaCroix, B.S., Trinity University;
M.S., Texas A&M University
Chair of Advisory Committee: Dr. Andrew McFarland

A two -stage circumferential slot virtual impactor aerosol concentrator system has been developed that is designed for nominal operational conditions of a 2 μm AD cutpoint, an aerosol inflow to the first stage of 100 L/min and a minor flow rate from the second stage of 1 L/min. Each unit was tested separately before being combined in the system. However, because of high inter-stage losses, a sheath air system was inserted between the two stages, wherein a small amount of air was injected into the apex of a cone placed on top of the second stage. The sheath air displaced the stagnation point at the apex of the cone and redirected particles into the sampling zone of the second stage unit. The cutpoint particle size of the system was 2.5 μm AD at the nominal flow rate. The dynamic range (ratio of upper limit to the lower limit of aerodynamic particle diameter associated with transmission efficiencies of 50%) was 5.4, and the largest particle size for which the transmission was at least 50% is 13.6 μm AD. When run at 67 L/min, the cutpoint is 4 μm AD and the dynamic range is 3.75; at 150 L/min the cutpoint is 2.05 μm AD and the dynamic range is not less than 4.74. The pressure drop across the system is 685 Pa (2.75 in. H2O). This yields an ideal power consumption of 0.77 watts.

TABLE OF CONTENTS

Page

LIST OF FIGURES

Page

LIST OF TABLES

Page

1. INTRODUCTION

The near-real time detection of bioaerosol particles is often limited by concentration considerations. Normal background bioaerosol concentration in buildings and the ambient environment is on the order of one ACPLA (agent containing particle per liter of air), U.S. National Academy of Sciences (2005). The typical view volume of a fluorescent bioaerosol detector can accommodate a flow rate of about 1 L/min (e.g., a Model 3317 Fluoresce Aerosol Particle Sensor TSI Incorporated, Shoreview, MN), which suggests that if the aerosol were concentrated by a factor of 100, near-background levels of a bioaerosol could be detected more rapidly and with greater reliability.

Most near-real-time bioaerosol detection systems consist of an inlet, a concentrator, and a sensing system. The inlet allows specific particle sizes to penetrate the system while keeping out unwanted debris. An effective concentrator will greatly reduce the air flow rate and create a particle rich flow for the sensing system, which analyzes the aerosol. A slot virtual impactor is one type of concentrator that may be used. Slot virtual impactors work by sharply redirecting the majority of the air through what is typically a 90° angle, and allowing a small part of the airflow (typically 10% of the inlet flow) to proceed in the forward direction as shown in Figure 1. The air that flows through the 90° angle is referred to as the major flow, and the air that proceeds in the forward direction is the minor flow. While air and smaller particles can make a 90° turn, the larger particles cannot and so they are separated from the major flow and proceed with the minor flow in the forward direction. For the typical single stage virtual impactor design, the separation ideally results in a ten times increase in the concentration of bioaerosol particles in the minor flow stream. A two-stage impactor repeats the process twice with two units placed in series. For the system considered herein, the first stage would concentrate the aerosol particles in a flow rate of 100 L/min into a flow rate of 10 L/min, while the second stage unit would concentrate the particles in the 10 L/min

---

This thesis follows the style of *Aerosol Science and Technology*.

minor flow from the first stage into a flow rate of 1 L/min. If this is done effectively, there is virtually no loss in particles as flow is reduced from 100 L/min to 1 L/min. This would translate to a theoretical concentration of large-sized particles that is 100 times that of the original sample.

The minor flow aerosol transmission of a virtual impactor is, for a given particle size, the fraction of those particles that are exhausted with the minor flow to those that enter the device. Typically the performance of a virtual impactor is presented in terms of a curve showing transmission as a function of aerodynamic particle diameter or Stokes number, with the curve having in inverted U-shape, Hari et al. (2007). Figure 15 of this document, shows a typical example of this curve shape. The cutpoint size of a virtual impactor is the smaller aerodynamic particle diameter at which transmission equals 50%. Correspondingly, cutpoint may also be represented as the Stokes number at which transmission equals 50%. There is another, larger particle size, at which transmission falls to 50%. The dynamic range of a concentrator, as reported herein, is the ratio of these latter two particle aerodynamic particle diameters.

The power needed to operate a virtual impactor is a factor that is of concern for field applications, where the device may be battery powered. The ideal power consumption (neglecting energy losses in blower and motor) can be represented by:

$$\dot{W}_{Ideal} = \sum Q_i \Delta P_i \qquad [1]$$

A high flow rate along with a high pressure drop translates to high power consumption. Because the flow rate is fixed, the best way to reduce the power necessary to operate the concentrator is to have small pressure drops across all of the flow pathways. A single stage unit operating at 100 L/min has a pressure drop of 40 Pa (0.16 in H2O) across the major flow pathway and an ideal power need of 0.14 watts (Haglund and McFarland 2004).

2. THEORY AND BACKGROUND

There are three main parameters used in characterizing the performance of a virtual impactor. The first parameter, the Stokes number (Stk), is defined as:

$$Stk = \frac{\rho_w D_a^2 C_c U_0}{18 \mu L_c} \qquad [2]$$

The parameters that comprise the Stokes number are listed in the Nomenclature section of this document. The Stokes number for an impactor is the ratio of the stopping distance for a particle at the average exit velocity to the half width of the jet (the critical dimension). It also represents the ratio of the inertial and drag forces acting on a moving particle. The lower the value of Stk, the more likely the particle will follow the curvilinear streamlines of air. Conversely, a particle with a higher value of Stk will deviate from the air streamlines in a flow field with non-linear streamlines. The diameter of the particle used in this calculation is known as the aerodynamic particle diameter (AD). That is, the diameter of a particle with unit specific gravity with the same gravitational terminal velocity as the particle tested.

The second parameter is the minor flow fraction (f), which is the ratio of the air volumetric flow rate at the minor flow rate exhaust port to the total flow rate (major plus minor) that enters the virtual impactor. Typically, virtual impactors are designed to operate with f =10%; however, they can be operated over a range of minor flow fractions from 5% to 20% (Seshadri, 2007).

The third parameter is the Reynolds number (Re), which is used to characterize the flow of the air.

$$\mathrm{Re} = \frac{\rho_f U_0 L_c}{\mu} \qquad [3]$$

The Reynolds number is the ratio of inertial forces to viscous forces in the air flow. When inertia forces are comparatively small, the flow is laminar. Conversely, when the

inertia forces are high, the flow is turbulent. For a Newtonian fluid such as air, laminar flow has smooth streamlines and layers and is more reliably modeled due to the linear shear stress it experiences, Fox et al. (2004). The effect of Reynolds number on the performance of the virtual impactors was not investigated in this study. For the first and second stages, the Reynolds numbers based on slot widths and nominal intake flow rates of 100 and 10 L/min, respectively, were 994 and 235. These Reynolds number can be considered to be in the laminar flow range.

The performance of a virtual impactor is typically presented in terms of the transmission of coarse particles from the inlet of the impactor to the exit plane of the minor flow. Transmission in terms of experimentally measured variables is:

$$T_{meas} = \frac{\left(\frac{F_s V_s Q_s}{t_s}\right)}{\left(\frac{F_r V_r Q_r}{t_r}\right)} \qquad [4]$$

The transmission of a concentrator having a fixed geometry and operated with a fixed ratio of minor to total flow rate, is primarily a function of Stokes number and to a second order it is a function of the minor flow fraction and Reynolds number.

A high transmission over a broad spectrum of particle sizes is desired for a virtual impactor that is used in bioaerosol sampling. The dynamic range based on particle size, R_{AD}, is defined as:

$$R_{AD} = \frac{D_{a,U\,50}}{D_{a,\,50}} \qquad [5]$$

Here: $D_{a,50}$ is the cutpoint particle size and $D_{a,U50}$ is the upper limit of aerodynamic size for which the transmission is at least 50%. For particle sizes less than the cutpoint, particles more closely follow the streamlines of the flow and are primarily transported into the minor flow passage; however, some of the small particles are transported by the minor flow and exhausted with the coarse particles. For an ideal virtual impactor, the

transmission should approach 100% for large particles. However, due to losses of aerosol particles on internal surfaces, the typical maximum transmission of aerosol through a single virtual impaction stage is about 90% (Adams, 2006). This means that in a two-stage system the maximum transmission will be approximately 80% as the transmission of two virtual impaction stages placed in series will be the product of the individual transmission values. For particles above the $D_{a,U50}$, losses occur primarily because of a crossing trajectory effect (Hari et al, 2007).

The ideal power needed to draw air through a virtual impactor system, Equation 1, is dependent only on flow rate and the pressure drop. For the Two-Stage Circumferential Virtual Impactor system, pressure drops and flow rates across the four major flows and the single minor flow exhaust were measured, rendering an ideal power consumption of:

$$\dot{W}_{Ideal} = Q_{maj1}\Delta P_{maj1} + Q_{maj2}\Delta P_{maj2} + Q_{\min}\Delta P_{\min} + Q_{Sheath}\Delta P_{Sheath} \qquad [6]$$

The equation also includes the ideal power for a sheath air flow system, which is used in the combined unit to increase overall efficiency. It is discussed in more detail later.

3. LITERATURE REVIEW

Although Hounam and Sherwood (1965) were the first to publish material covering virtual inertial impaction, the background of the work can more directly be linked to Conner (1966), who devised and tested a system comprised of circular acceleration and receiver nozzles. For a unit operated at a flow rate of 40 L/min, he used polystyrene latex particles to determine a cutpoint of 1.4 μm, and achieved a transmission greater than 90% for a range of particles.

Theoretical understanding of virtual impactors has been advanced by several studies. Forney et. al. (1978) modeled a virtual impactor using a two-dimensional ideal fluid and compared the results with experimental data. Keeping a fixed Reynolds number, Forney was able to achieve good agreement between theoretical predictions and experimental results. Forney et al. (1982) was able to expand previous findings to include the effects of throat angle and normalized slot width on performance. The experimental results had trends that matched well with more advanced theoretical models based upon the Navier-Stokes equations. Chen et al. (1985) studied the effects of Reynolds number as well as the effects of adjusting the minor flow rate ratio.
Loo and Cork (1988) stated two principles based upon their development of a single stage virtual impactor. The first is that internal dimensions of an impactor should be adjusted based upon theoretical knowledge of impaction theory. The second is that symmetry is important. This leads to a sharper cutpoint as well as lower internal wall losses.

Numerical simulations of virtual impactors have also been conducted. Marple did the first numerical modeling of the virtual impactor (Marple and Chien 1980). More recently, Lin and Heintzenberg (1995) used a three-dimensional axis-symmetric potential flow model to simulate a counterflow virtual impactor. Their results matched well with experimental data. Asgharian and Godo (1997) used flow field information calculated from finite element analysis as well as the governing equations of motion of spherical particles to calculate transmission and losses in an impactor experimentally tested by Chen and Yeh (1987). Hu and McFarland (2007) analyzed flow instabilities in

the two stages of the virtual impactor investigated herein and developed design modifications to rectify the instabilities. Flow instabilities in the first stage had caused a serious degradation of performance.

Directly relevant to the present study is the work of Haglund and McFarland (2004), who developed the design for the circumferential slot virtual impactor (CSVI) that served as the foundation for the units employed in this study. Hari (2003) was able to model the CSVI, and his simulations matched the experimental results of Haglund and McFarland. Isaguirre (2004) developed a two-stage unit that had a peak transmission of 95% and a dynamic range based on particle size of 5. The most recent CSVI work is that of Adams (2006), who collaborated with TSI Inc (Shoreview, MN,) to design a CSVI with a nominal flow rate of 10 L/min. The unit has a dynamic range of 10.9.

4. DESIGN

The completed and assembled Two-Stage CSVI is shown in Figure 2. Figures 3 and 4 show the disassembled first stage unit and the assembled second stage unit, respectively. The principal dimensions of the first and second stage units were based upon numerical simulations by Hu and Hari (Adams et al. 2006). Each unit has consistent laminar flow through the unit at its respective flow rate. The goal of this project is to integrate the two stages and maintain stable, laminar flows, without a significant decrease in the dynamic range. Both units have parabolic entrance sections that help reduce crossing particle trajectories (Hari, 2007) in the critical zone, thus increasing the effective dynamic range of each unit.

The first stage unit is designed to operate at 100 L/min and has been integrated into the structure of the upper plenum, as seen in Figure 3. There are three 6.22 mm (0.245") supports that hold the top of the first stage to the lower assembly. The plenum has an inner diameter of 127 mm (5"). The concave bottom of the plenum is important in the design from the standpoint of achieving effective aspiration of particles into the critical zone of the first stage. Prior to entering the 1st stage acceleration nozzle, some flow streamlines go below the level of the entrance slot and then bend back to the acceleration nozzle. The acceleration nozzle has a width of 0.711 mm (0.028"). Past the critical zone there is a cusp that acts to direct flow towards the minor flow exhaust tube. The second stage unit, which has been reduced in size from that of Adams (2006), can be seen in Figure 4. The overall height has been reduced from 86.4 mm to 76.2 mm (3.4" to 3"). The critical zone measurements have not been changed, e.g., the acceleration nozzle width is still 0.35 mm (0.014").

During initial efforts to integrate the first and second stage units, severe losses were encountered when the units were coupled. The minor flow exhausted from the first stage is a concentrated beam of particles. These particles can be impacted, or sedimented, on the body of the second stage unit thus greatly reducing overall transmission. To counteract this effect, an independent study was done, Hu et al. (2007),

which resulted in the implementation of a cone with sheath air, where the sheath air was exhausted from the apex of the cone.

The cone, which has a height 30.5 mm (1.2”) is placed on top of the second stage unit as can be seen in Figures 4 and 5. The cone has a 1.59 mm (1/16 “) diameter hole at the apex. Air is pumped out of the hole at a low flow rate (1-2% of the flow rate entering the second stage, or 0.1 – 0.2% of the total flow rate entering the first stage of the two-stage system). This air stream displaces the stagnation point of the particles as can be seen in Figure 5. The combination of the cone and sheath air can increase overall transmission by as much as 86% for 10 μm particles in a two-stage system (Hu et al, 2007).

The power necessary to operate the sheath air system is very low. For the 100 L/min system, the sheath air rate is 0.2 L/min and the pressure drop is less than 25 Pa (0.1 inch of H2O). This results in an ideal power consumption that is extremely low (10-5 watt) and is thus neglected in the calculation of ideal power for the CSVI system.

5. METHODOLOGY

Two experimental procedures are used in this study. The first is measurement of aerosol sampling performance; which involves the generation, collection, and analysis of aerosol particles. The second is measurement of pressure.

Regarding aerosol sampling performance, the overall concept is to generate aerosol particles of a specific size and a constant concentration at a given flow rate, and to sample these particle before and after passage through a CSVI unit. The particles that pass through a unit are collected on filters at each of the exit ports and later analyzed. To provide reference samples, the process is repeated with the same size particles, the same concentration and the same flow rate for the same amount of time, with the sampling taking place directly on a filter without a virtual impactor in place. The comparison of the particle mass collected by the filter on the minor flow of the unit and the reference filter gives the transmission of the unit.

Particles with a diameter less than 3 μm AD are generated by atomization of liquid suspensions of fluorescently-tagged polystyrene spheres (PSL, Duke Scientific, Palo Alto, CA). The spheres are aerosolized with a six-jet collision nebulizer (Model CN311, BGI Inc., Waltham, MA). The PSL hydrosol from the vendor is diluted with water to form a master suspension with a concentration no higher than 10^9 particles/mL (the concentration beyond which there will be an unacceptably high concentration of aerosol particles comprised of two or more polystyrene spheres). For each test, 60 mL of PSL suspension is put in the nebulizer and then the atomizer is subjected to a flow of pressurized air (100 – 200 kPa). After each test, the liquid in the nebulizer is emptied into a transfer vessel and the nebulizer is refilled with another 60 mL of the master suspension. During the tests, the master suspension is stirred with a magnetic rod to keep it uniformly mixed. At the conclusion of a set of tests, the transfer vessel containing the used suspension is combined with the leftover master suspension and stored in a sealable glass bottle to be reused in the future. A schematic diagram, showing the setup employed for the PSL tests, is given in Figure 6, while the reference set-up can be seen in Figure 7.

It should be noted that the PSL are not sized by aerodynamic particle diameter. Equation 7 shows the calculation used to find the AD.

$$D_a = D_{PSL}\sqrt{\frac{\rho_{PSL}}{\rho_W}} \qquad [7]$$

Particles sizes larger than 3 μm are generated with a vibrating orifice aerosol generator (VOAG) (Model 3450, TSI Inc., Shoreview, MN). The test aerosol particles are created from atomization of a solution of oleic acid, ethanol, and a fluorescent tag, sodium fluorescein, followed by the subsequent evaporation of the ethanol to form residual test droplets of fluorescently-tagged oleic acid. Before use, a master solution of 90% ethanol, 9% oleic acid, and 1% sodium fluorescein is diluted with ethanol to achieve the desired droplet size. The size of the residual test droplets can be estimated from:

$$D_d = \left(\frac{6Q_{VOAG}C_{Vol}}{\pi\ f_{VOAG}}\right)^{\frac{1}{3}} \qquad [8]$$

and

$$C_{vol} = \frac{x_{fr}V_m}{V_m + V_d} \qquad [9]$$

During a test, the concentration and size distribution of the aerosol is monitored with an Aerodynamic Particle Sizer (APS, Model 3321, TSI, St. Paul, MN). A monodispersed aerosol with constant concentration is desired. If the particles being generated are not monodispersed, the VOAG frequency is adjusted until monodispersity is achieved. According to the manufacturer, the resolution for the particle sizer is .02 μm for 1 μm particles and .03 μm for particles greater than 10 μm. Monodispersity for oleic acid particles is defined as limiting particle range to four adjacent particle sizes according to the particle sizer. If the concentration does not stay constant throughout the test, then the test is aborted and must be re-run.

The size of the particles generated with the VOAG is determined with the aid of a microscope. The liquid particles are impacted on a glass slide coated with an oil-phobic chemical (NyeBar Type Q 2.0%, W.F. Nye Lubricants Inc., New Bedford, MA). They are then viewed at 400X magnification under a microscope (Ellipse E600, Nikon, Tokyo, Japan) and a picture is taken with a digital camera (CoolSNAP, Photometrics, Tuscon, AZ). The particles are then measured digitally using a commercially-available software program (Metamorph, Universal Imaging Corp., Downingtown, PA). The particle size observed under the microscope is adjusted for flattening using a factor of 1.29 (Olan-Figureoa et. al., 1982,: Thien, 2004). Additionally, oleic acid has a different density than water. The particle size is presented as a function of AD, where the relationship between measured droplet size, flattening factor, density and aerodynamic particle diameter is:

$$D_a = \frac{D_{meas}}{F_f}\sqrt{\frac{\rho_b}{\rho_w}} \qquad [10]$$

A schematic diagram of the apparatus used to test the CSVI units with oleic acid aerosol particles is shown in Figure 8. The flow rates in the two major flow exhaust lines are measured with identical mass flow meters (Model 4045, TSI Inc., St. Paul, MN) while the minor flow rate is measured with a smaller-sized mass flow meter (Model 4143, TSI Inc., St. Paul, MN). Each flow rate can be adjusted independently. The particles are collected on glass fiber filters (Type A/D glass fiber filters, PALL, East Hills, NY), which are located upstream of the flow meters. The system is typically run for 10-15 minutes, and the filters are changed every five minutes to obtain 2 or 3 replicate samples. Directly following the conclusion of sample acquisition with the CSVI device, it is removed and replaced with a reference filter system, which is operated at the same flow rate for the same amount of time. The reference filter installed in the test apparatus is illustrated in Figure 9. The filters from each test are collected and stored in separate glass containers.

The fluorescent tag in the particles deposited on the filters is then eluted. For PSL particles this involves adding 10-20 mL of ethyl acetate and soaking the filter for a minimum of one hour. The filters from VOAG tests, where the aerosol particles are tagged with sodium fluorescein, are soaked in equal parts isopropyl and distilled water for a minimum of 6 hours. Approximately 6-7 mL of the liquid are placed into a 12 × 75 mm glass culture tube. Prior to fluorometric analysis (FM109515, Barnstead International, Dubuque, IA), the solution is stabilized with three drops of one molar NaOH. The addition of the NaOH maximizes the fluorescence of fluorescein, which is pH sensitive (Kesavan et al., 2001). However, it also causes a slight dilution of the sample in a cuvette, which changes the volume of liquid in the cuvette by less than 2% on average.

The fluorometer requires two optical filters. The first filter is a low pass device that sets an upper limit on the excitation wavelength. The second is a high pass filter that sets a lower limit for the wavelength of emitted light that is allowed to reach a photodetector. It is necessary to change the filters according to the fluorescent substance being measured. The PSL suspensions are provided in three different sizes, with each size having a different color (red, blue, and green). Each size requires a different set of filters; however, by changing filters, it is possible to analyze each size even if all three sizes were generated simultaneously. The results for each particle size are recorded and compared to its corresponding reference to find the transmission. A sampling transmission of 100% means that all of the particles that are introduced into a unit are transmitted through the unit to the minor flow exhaust port.

The pressure drop across the unit is measured using the same basic flow set-up as shown in Figure 8. Over a range of flow rates from 50 L/min to 150 L/min, the pressure drop is measured across the major and minor flow paths with an inclined manometer (Durablock, Dwyer Instruments Inc., Michigan City, IN).

6. RESULTS AND DISCUSSION

6.1 *First Stage Unit*

The first stage unit operated has a Stokes cutpoint of 1.1 and when operated at a flow rate of 100 L/min, it has a cutpoint particle size of 2.4 μm AD, Figure 10. The maximum transmission is 93%. The dynamic range, based on particle size, is about 5.8 with consistent transmission ≥ 86% for sizes in the range of 3.0 to 13.8 μm AD. There is good agreement between the numerical simulation and experimental data. Figure 11 shows performance with and without the cusp; the implementation of which increased transmission by 14% to 18%. The data for the first stage unit operated independently are presented in Appendix A1.

6.2 *Second Stage Unit*

The second stage unit has a Stokes cutpoint of 1.2 and when operated at an inlet flow rate of 10 L/min, it has a cutpoint particle size of 2.5 μm AD with a maximum transmission of 94%, Figure 12a and Figure 12b. The unit has consistent transmission ≥ 90% for the size range of 4.1 to 14.5 μm AD and a dynamic range of at least 5.8. The figures also show the transmission curves for the second stage unit compared with results from numerical simulation (Hu, 2007). Similar to the first stage, there is good agreement between the numerical simulation and the experimental data. The data for the second stage unit operated independently are presented in Appendix A2.

6.3 *Combined*

When operated at an inlet flow rate of 100 L/min and a second stage minor flow rate of 1 L/min, the combined two-stage system has a particle size cutpoint of 2.5 μm AD and a maximum transmission of 88% for the size range of 2.5 to 13.6 μm AD, Figure 13. The dynamic range for the combined unit, based on particle size, is 5.4. Here, the results are not presented in terms of Stokes numbers because the two stages have different

relationships between transmission and Stokes number, which precludes representation of the combined system results with a single Stokes number.

In Figure 13, the "predicted" curve is the product of the transmission of the two units at a given particle size. Were it not for internal losses between the stages, the overall transmission at a given particle size for the combined system should equal the product of the transmission for each CSVI. Also shown is the transmission of the combined system without sheath air. At small particle sizes the lack of a sheath air system does not affect transmission. However, transmission is reduced at larger particle sizes when sheath air is not employed. The data for the combined unit are presented in Appendix A3.

Figure 14 shows the transmission efficiency for total inlet flow rates of 67 L/min and 150 L/min, with second stage minor flow rate of 1% of the first stage inlet flow rate, compared to the performance at 100 L/min. All three flow rates show similar peak performance numbers. However, when the unit is run at 150 L/min, the air velocities in the slots velocities are higher, thus the particle size at the cutpoint is reduced. The opposite effect can be seen in the 67 L/min performance curve, which has a larger cutpoint size due to the lower slot velocities. At the three flow rates of 150, 100 and 65 L/min, the cutpoint particle sizes are 2.05, 2.5, and 4.0 μm AD, respectively. Figure 15 shows the results using the Stokes numbers from the first stage unit to represent the overall system. There is good agreement between the results for the three different flow rates, which indicates that the fundamental performance does not change with minor changes in the overall flow rate. As a consequence, the cutpoints associated with off-design flow rates could be calculated from Stokes number considerations. The data for the 150 L/min and 67 L/ tests is presented in Appendix A4.

6.4 *Pressure Drop*

As stated previously, a CSVI with relatively low pressure drops across the unit could be operated without a major external power source. The pressure drop was measured for overall flow rates from 50 to 150 L/min. The results can be seen in Figure 16. When

operating at 100 L/min the ideal power consumption (computed using equation 6) is 0.77 watts. The total ideal power for the other flow rates can be seen in Figure 17. The data for the pressure drop measurements are presented in Appendix A5.

7. UNCERTAINTY ANALYSIS

In 1953, Kline and McClintock developed an uncertainty analysis based on single sample estimates, where the uncertainty in a dependent variable can be calculated from a priori estimates of the uncertainty in statistically independent variables, provided a functional relationship between the dependent and independent variables is known. The Kline-McClintock equation for uncertainty is:

$$\delta Z = \left[\sum_{i=1}^{n} \left(\frac{\partial Z}{\partial X_i} \delta X_i \right)^2 \right]^{\frac{1}{2}} \qquad [11]$$

The Stokes Number calculation and the transmission calculation will be considered herein from the uncertainty perspective. Equations 12 and 13 show the calculations for the Cunningham Correction factor and particle velocity respectively.

$$C_C = 1 + 2.52 \frac{\lambda}{D_P} \qquad [12]$$

$$U_0 = \frac{Q}{2 \cdot L_C \cdot \pi \cdot D_{CZ}} \qquad [13]$$

Substituted into the equation for Stokes number gives:

$$Stk = \frac{\rho_p D_p^2 Q \left(1 + 2.52 \frac{\lambda}{D_p} \right)}{36 \cdot \pi \cdot \mu \cdot L_C^2 \cdot D_{CZ}} \qquad [14]$$

The overall flow rate, the critical dimension (half acceleration nozzle slot width), and the particle diameter (D_p) are considered to be statistical random variables. The uncertainty of all other factors is considered inconsequential. Using equation 11, the uncertainty for each parameter can be characterized as:

$$\frac{\partial Stk}{\partial Q_s} = \frac{Stk}{Q_s} \qquad [15]$$

$$\frac{\partial Stk}{\partial L_C} = \frac{-2Stk}{L_C} \qquad [16]$$

$$\frac{\partial Stk}{\partial D_p} = \frac{Stk}{D_p}\left[\frac{2D_p + 2.52\lambda}{D_p + 2.52\lambda}\right] \qquad [17]$$

Thus the total uncertainty of the Stokes number calculation is:

$$\delta Stk = Stk\left[\left(\frac{\delta Q_s}{Q_s}\right)^2 + \left(\frac{-2\delta L_C}{L_C}\right)^2 + \left(\frac{\delta D_p}{D_p}\left\{\frac{2D_p + 2.52\lambda}{D_p + 2.52\lambda}\right\}\right)^2\right]^{\frac{1}{2}} \qquad [18]$$

Assuming the relative uncertainty in flow rate and slot width are 2% and 0.5%, respectively, the overall uncertainty can be expressed as a function of particle diameter, viz:

$$\frac{\delta Stk}{Stk} = \left[(0.02)^2 + (-2\cdot(0.005))^2 + \left(0.03\left\{\frac{2D_p + 2.52\lambda}{D_p + 2.52\lambda}\right\}\right)^2\right]^{\frac{1}{2}} \qquad [19]$$

Over the range of particle sizes tested, the maximum error is ±6%.

A similar calculation can be done with the transmission calculation. Assuming that error in time measurement is inconsequential and that the sample times were equal, the transmission in terms of measured parameters can be characterized by:

$$T = \frac{Q_s V_s F_s}{Q_r V_r F_r} \qquad [20]$$

Using the Kline-McClintock equation as above, the uncertainty is:

$$\delta T = T\left[\left(\frac{\delta Q_s}{Q_s}\right)^2 + \left(\frac{-\delta Q_r}{Q_r}\right)^2 + \left(\frac{\delta V_s}{V_s}\right)^2 + \left(\frac{-\delta V_r}{V_r}\right)^2 + \left(\frac{\delta F_s}{F_s}\right)^2 + \left(\frac{-\delta F_r}{F_r}\right)^2\right]^{\frac{1}{2}} \quad [21]$$

The relative uncertainties are listed in Table 1. The resulting equation is:

$$\frac{\delta T}{T} = \left[(0.025)^2 + (0.025)^2 + (0.01)^2 + (0.01)^2 + \left(\frac{\delta F_s}{F_s}\right)^2 + \left(\frac{-\delta F_r}{F_r}\right)^2\right]^{\frac{1}{2}} \quad [22]$$

The error is now a function of the sample and reference fluorometer readings for each test run. The minimum and maximum errors are ±3.5% and ±13.2% respectively.

Uncertainty for the PSL particle diameters is based upon the manufacturer's specifications. For all sizes used, the diameters are ±5% of the listed size. Oleic acid particle diameter uncertainty is based upon the monodispersity defined earlier. A maximum of four registered sizes was permitted for each test. Each registered size is 0.03 μm different; this gives a range of 0.12 μm for any given size. The minimum and maximum errors for oleic acid particle diameter are ±1% and ±5% respectively.

8. SUMMARY AND CONCLUSION

A two-stage circumferential slot virtual impactor has been constructed and tested. The units were developed independent of this study, but were tested herein both separately and as a two-stage integrated system. The first stage has a cutpoint Stokes number of 1.2 and a cutpoint particle size of 2.5 μm AD, and a transmission of at least 89% for particles up to 13.5 μ AD (Stokes number of 36); the maximum transmission is 93% for a 10.1 μm AD particle (Stokes number 19.5). The second stage has a cutpoint Stokes number of 1.2 and a cutpoint particle size of 2.5 μm AD, and a transmission of at least 91% for particles up to 14.5 μm AD. The maximum transmission is 93% for a 4.1 μm AD particle size.

When the two stages were combined in series, there were large losses observed on the top of the second stage unit. To counteract this, a small cone was added along with the introduction of a counter flow stream that is 1-2% of the flow rate into the second stage. The combined unit has a cutpoint of 2.5 μm AD, and a peak transmission of 88%, which occurs at a particle size of 5.8 μm AD. The dynamic range, of the combined system is 5.4 based on aerodynamic particle diameter.

The combined unit has also been run at flow rates of 67 and 150 L/min. At 67 L/min, the cutpoint is 4 μm AD and the dynamic range is 3.75. Peak transmission is 82% at a particle size of 4.83μm AD. When operated at 150 L/min, the cutpoint is 2.05 μm AD and the dynamic range is no less than 4.74. Maximum transmission is 85% at a particle size of 6.19 μm AD.

The pressure drop across the combined unit was measured at various flow rates. This measurement was then used to calculate the ideal power necessary to operate the CSVI. The pressure drop across the system at a flow rate of 100 L/min is 685 Pa (2.75 in. H2O), which yields an ideal power consumption of 0.77 watts.

NOMENCLATURE

C_c	=	The Cunningham correction factor (for particle slip)
C_{vol}	=	Volume fraction of oleic acid and fluorescein in ethanol
D_a	=	Aerodynamic particle diameter
$D_{a,50}$	=	Aerodynamic particle diameter cutpoint
$D_{a,U50}$	=	The upper limit aerodynamic particle diameter where transmission drops below 50%
D_{CZ}	=	Diameter of the critical zone
D_d	=	Diameter of droplets formed by VOAG
D_{meas}	=	Diameter of particle measured by microscope.
F_f	=	Flattening factor
F_s	=	Fluorometer reading from a sample collected downstream of a CSVI
F_r	=	Fluorometer reading from a reference sample
f_{VOAG}	=	Vibrating orifice aerosol generator frequency
L_c	=	Critical dimension
Q_i	=	Flow rate through a passage in the CSVI
Q_{maj1}	=	Flow rate through the major flow passages in the first stage CSVI
Q_{maj2}	=	Flow rate through the major flow passages in the second stage CSVI
Q_{minor}	=	Flow rate through the minor flow passages in the CSVI
Q_r	=	Flow rate of the reference sample used in experimentation
Q_s	=	Flow rate into the CSVI
Q_{sheath}	=	Flow rate of the sheath air
Q_{VOAG}	=	Solution flow rate in the Vibrating Orifice Aerosol Generator
R_{AD}	=	Dynamic range based on aerodynamic diameters
Re	=	Reynolds number
Stk	=	Stokes number
t_r	=	Duration of time a reference is run

t_s = Duration of time a CSVI sample is run

T = Transmission of aerosol particles of a given size through a virtual impactor. For a given particle size it is the ratio of aerosol particle mass flow rate at the minor flow exhaust port to aerosol particle flow rate at the inlet of the device.

V_s = Volume of the solvent used to elute tracer from an experimental sample

V_r = Volume of the solvent used to elute tracer from a reference sample

x_{fr} = Fraction of ethanol in master solution

X_i = Independent random variable used in Kline and McLintock estimation of uncertainty δZ of a dependent random variable,

U_0 = Mean velocity at the acceleration nozzle exit plane

V_d = Volume of the dilution ethanol

V_m = Volume of master solution

$\dot{W}_{Ideal}$ = Ideal power consumption of a CSVI

Z = Dependent statistical random variable in method of Kline and McClintock

ΔP_i = Pressure drop across a passage in the CSVI

ΔP_{maj1} = Average Pressure drop across the major flow passage in the first stage CSVI

ΔP_{maj2} = Average Pressure drop across the major flow passages in the second stage CSVI

ΔP_{minor} = Pressure drop across the minor flow passage in the CSVI

ΔP_{sheath} = Pressure drop for sheath air system

δ = Differential as used in the Kline and McClintock method for estimation of uncertainty

λ = Mean free path of air molecules

μ = Fluid dynamic viscosity

ρ_b = Density of oleic acid

ρ_f = Density of the fluid (air) entering the CSVI

ρ_p = Particle density

ρ_{PSL} = Density of PSL

ρ_w = Density of water

REFERENCES

Adams, C.W. (2006). Circumferential Slot Virtual Impactor for Bioaerosol Concentration. M.S. Thesis, Department of Mechanical Engineering, Texas A&M University, College Station, TX.

Adams, C.W., Hari, S., Hu, S., Thien, B.F., and McFarland, A.R.(2006). 100 L/min Circumferential Slot Virtual Impactor. Presentation at RDECOM Meeting, Applied Research Laboratories, University of Texas, Austin, TX, March 2006.

Asgharian, B. and Godo, M.N. (1997). Transport and Deposition of Spherical Particles and Fibers in an Improved Virtual Impactor, *Aerosol Sci. and Technol*. 27:499-506.

Chen, B.T., Yeh, H.C., and Cheng, Y.S. (1985). A Novel Virtual Impactor: Calibration and Use. *J. Aerosol Sci*. 16:343-354.

Chen, B. T. and Yeh, H.C. (1987). An Improved Virtual Impactor: Design and Performance, *J. Aerosol Sci*. 18:203-214.

Conner, W.D. (1966) An Inertial-Type Particle Separator for Collecting Large Samples, J. *Pollut Control Assoc*.16:35.

Forney, L.J., Ravenhall, D.G. and Winn, D.S. (1978). Aerosol Impactors: A Study of Fluid Jet Impinging Upon a Void, *J. Applied Phys*. 49: 2339.

Forney, L.J., Ravenhall, D.G. and Winn, D.S. (1982). Experimental and Theoretical Study of a Two-Dimensional Virtual Impactor, *Environ. Sci. & Technol*. 16:492-497.

Fox, R.W., McDonald, A.T. and Pritchard, P.J. (2004) *Introduction to Fluid Mechanics*. 6th ed. John Wiley and Sons, Hoboken, NJ p. 39.

Haglund, J. S. and McFarland, A. R. (2004). A Circumferential Slot Virtual Impactor, *Aerosol Sci. Technol*. 38: 664-674.

Hari, S. (2003). Two Computational Fluid Dynamics (CFD) Simulations of Dilute Fluid-Particle Flows. Ph.D Dissertation, Department of Nuclear Engineering, Texas A&M University, College Station, TX.

Hari, S., McFarland, A.R., Hassan Y.A. (2007). CFD Study on the Effects of the Large Particle Crossing Trajectory Phenomenon on Virtual Impactor Performance, *Aerosol Sci. Technol.* 41:1040–1048.

Hounam, R. F. and Sherwood, R. J. (1965). The Cascade Centripeter: A Device for Determining the Concentration and Size Distribution of Aerosols, *Am. Ind. Hyg. Assoc. J. 2*:122-131.

Hu, S. and McFarland, A.R. (2007). Circumferential Slot Virtual Impactors with Stable Flow. Aerosol Technology Laboratory Report 1007-6024. Dept of Mechanical Engineering, Texas A&M University, College Station, TX.

Hu, Shishan, LaCroix, D.E. and McFarland, A.R. (2007). Control of Particle Losses on a Cone by Stagnation Point Displacement with Sheath Air. Department of Mechanical Engineering, Texas A&M University, College Station, TX.

Isaguirre, R. (2004). A Two-Stage Circumferential Slot Virtual Impactor for Bioaerosol Concentration. M.S. Thesis, Department of Mechanical Engineering, Texas A&M University, College Station, TX.

Kesavan, J., Doherty, R. W., Wise, D. G. and McFarland, A. R. (2001). Factors That Affect Fluorescein Analysis. Edgewood Chemical Biological Center, U.S. Army Soldier and Biological Chemical Command Edgewood, MD. ECBC-TR-208.

Kline, S. J., and McClintock, F.A. (1953). Describing Uncertainties in Single-Sample Experiments, *Mech. Eng*. 73:3-8.

Lin, H. and Heintzenberg, J. (1995). A Theoretical Study of the Counterflow Virtual Impactor. *J. Aerosol Sci*. 26:903-914.

Loo, B. W., and Cork, C. P. (1988). Development of High Efficiency Virtual Impactors, *Aerosol Sci. Technol*. 9:167-176.

Marple, V. A., and Chien, C.M. (1980). Virtual Impactors: A Theoretical Study, *Environ. Sci. & Technol*. 14:976-985.

Olan-Figueroa, E., McFarland, A. R., Ortiz, C. A. (1982) Flattening Coefficients for DOP and Oleic Acid Droplets Collected on Treated Glass Slides, *Am. Ind. Hyg. Assoc. J.* 43: 395-399.

Seshadri, S. (2007) The In Line Virtual Impactor. Ph.D. Dissertation, Department of Mechanical Engineering, Texas A&M University. College Station, TX.

Thien, B. (2004). Flattening Factor for Oleic Acid Particles. Aerosol Technology Lab, Texas A&M University, College Station, TX.

U.S. National Academy of Science (2005). *Sensor Systems for Biological Agent Attacks: Protecting Buildings and Military Bases*. The National Academies Press, Washington D.C.

APPENDIX A

Table 1: Uncertainty values for the listed parameters

Parameter	Uncertainty
Qs	± 2.5%
Qr	± 2.5%
Vs	± 1%
Vr	± 1%

APPENDIX B

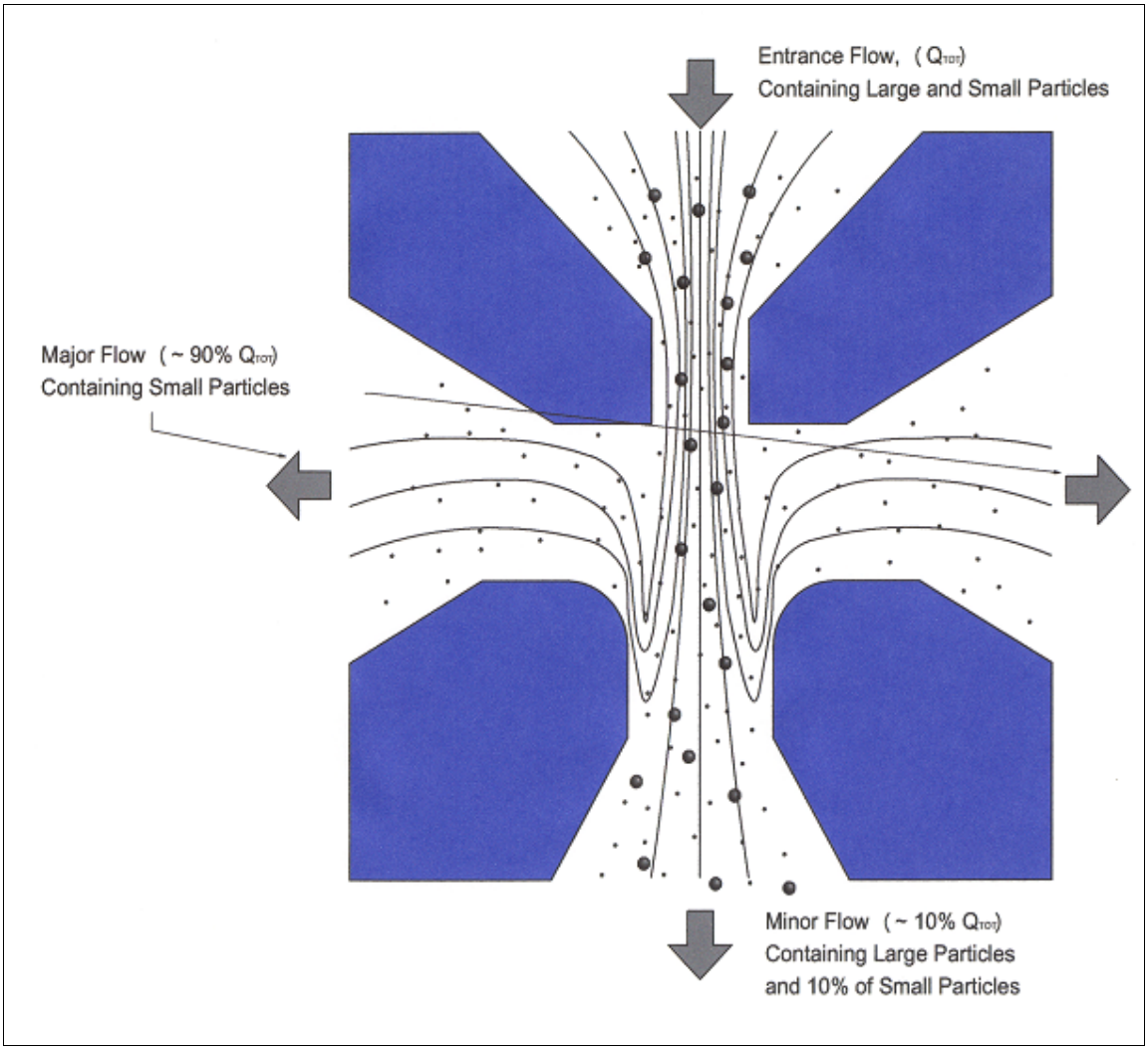

FIG. 1. An illustration of the virtual impaction concept.

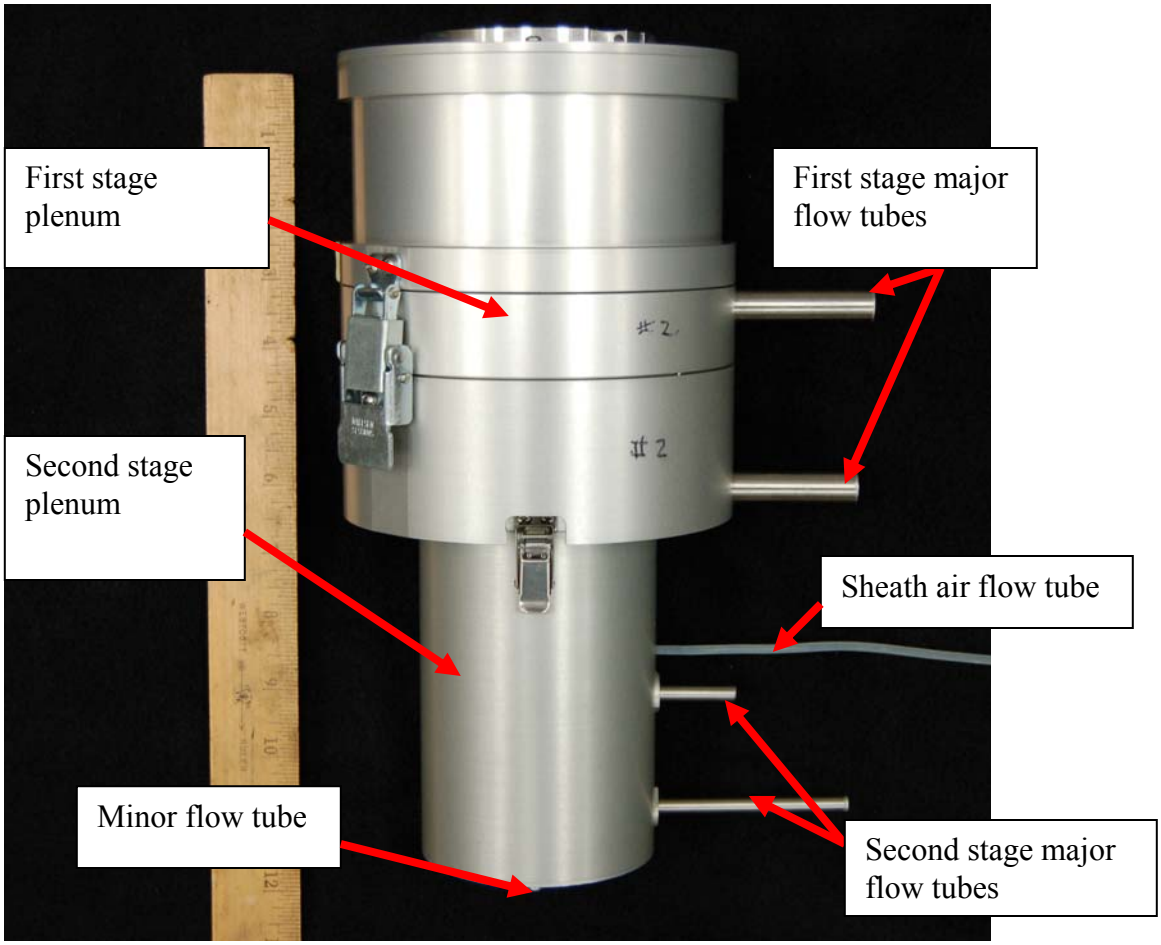

FIG. 2. Two-Stage 100 L/min circumferential slot virtual impactor.

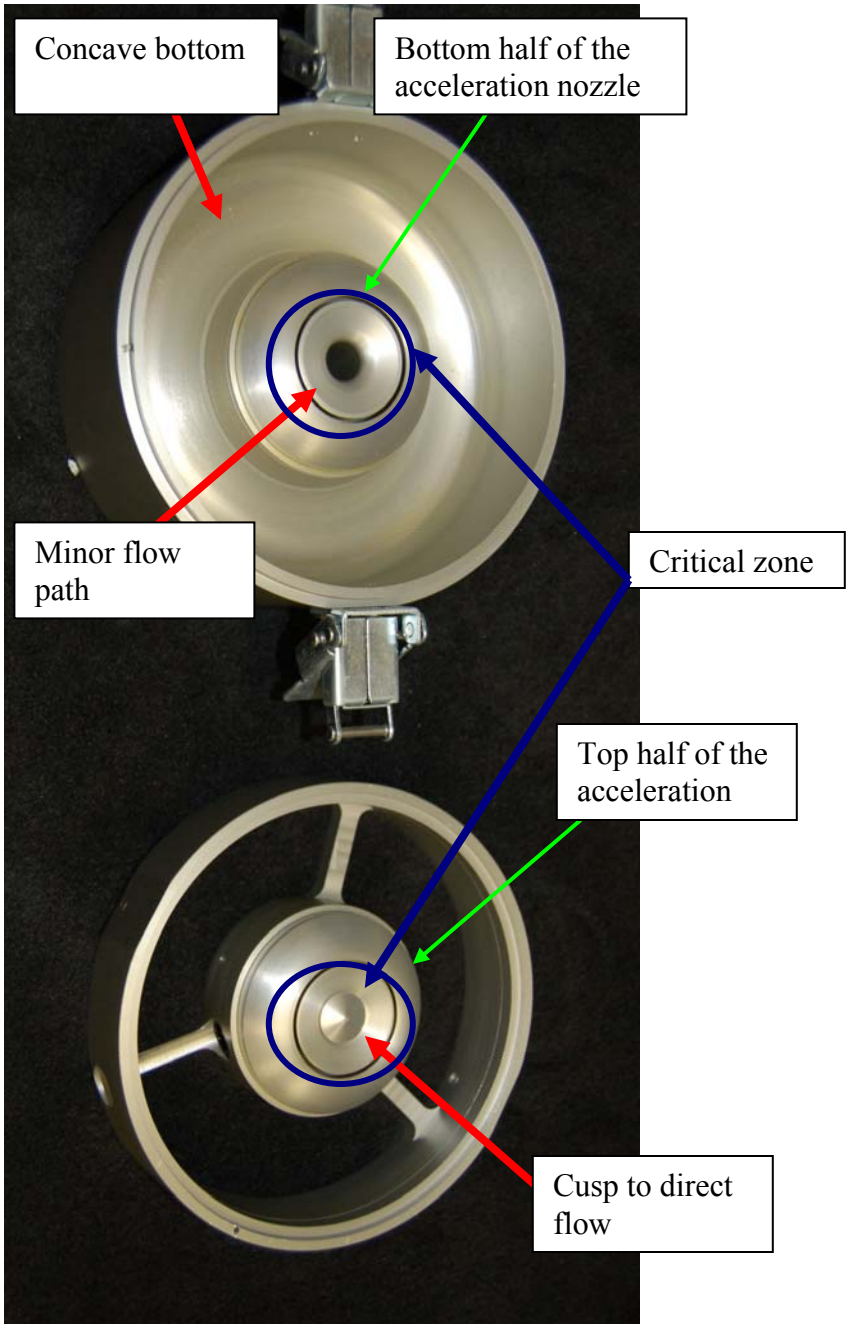

FIG. 3. Separated first stage unit.

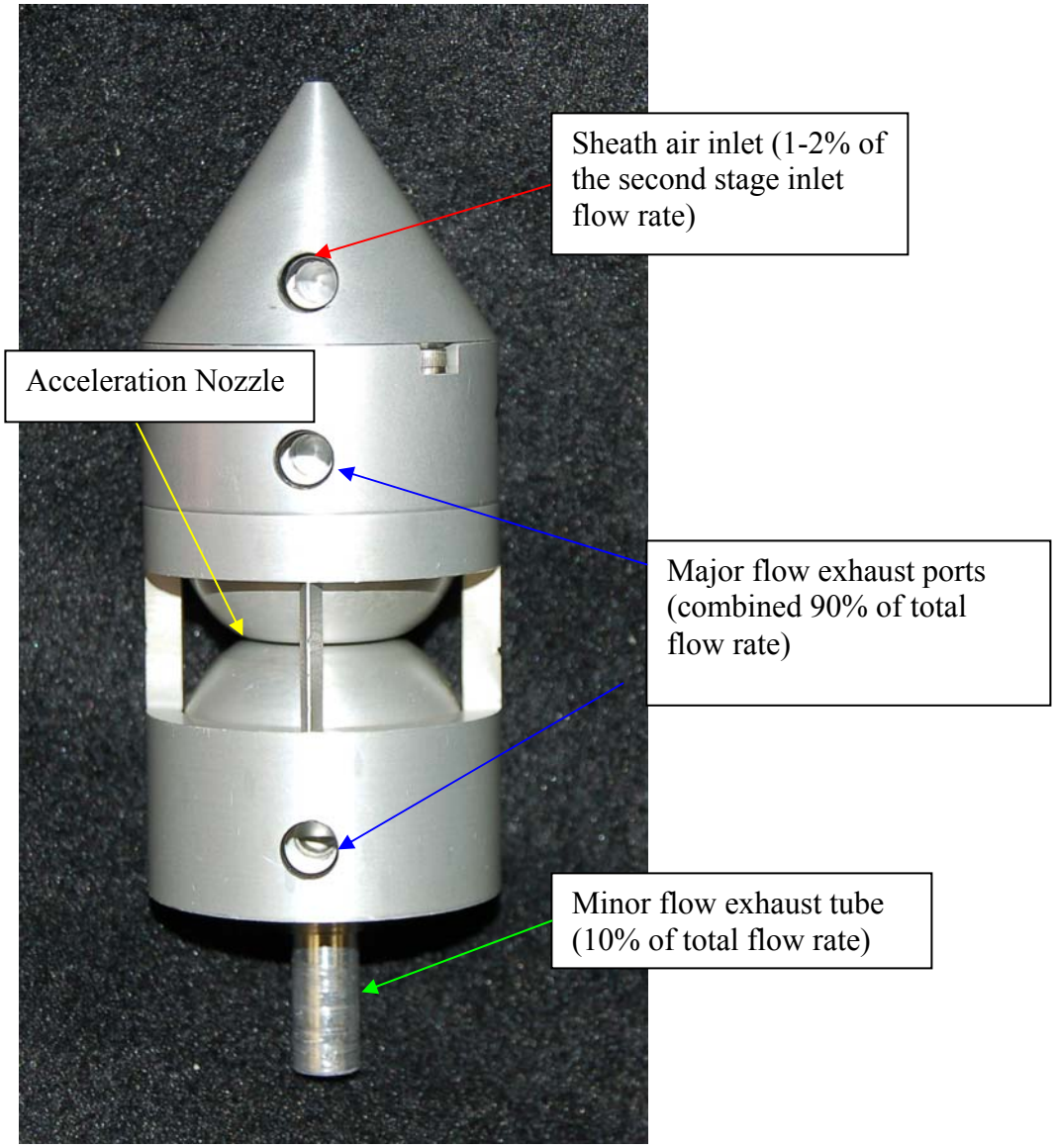

FIG. 4. Second stage unit with sheath air cone.

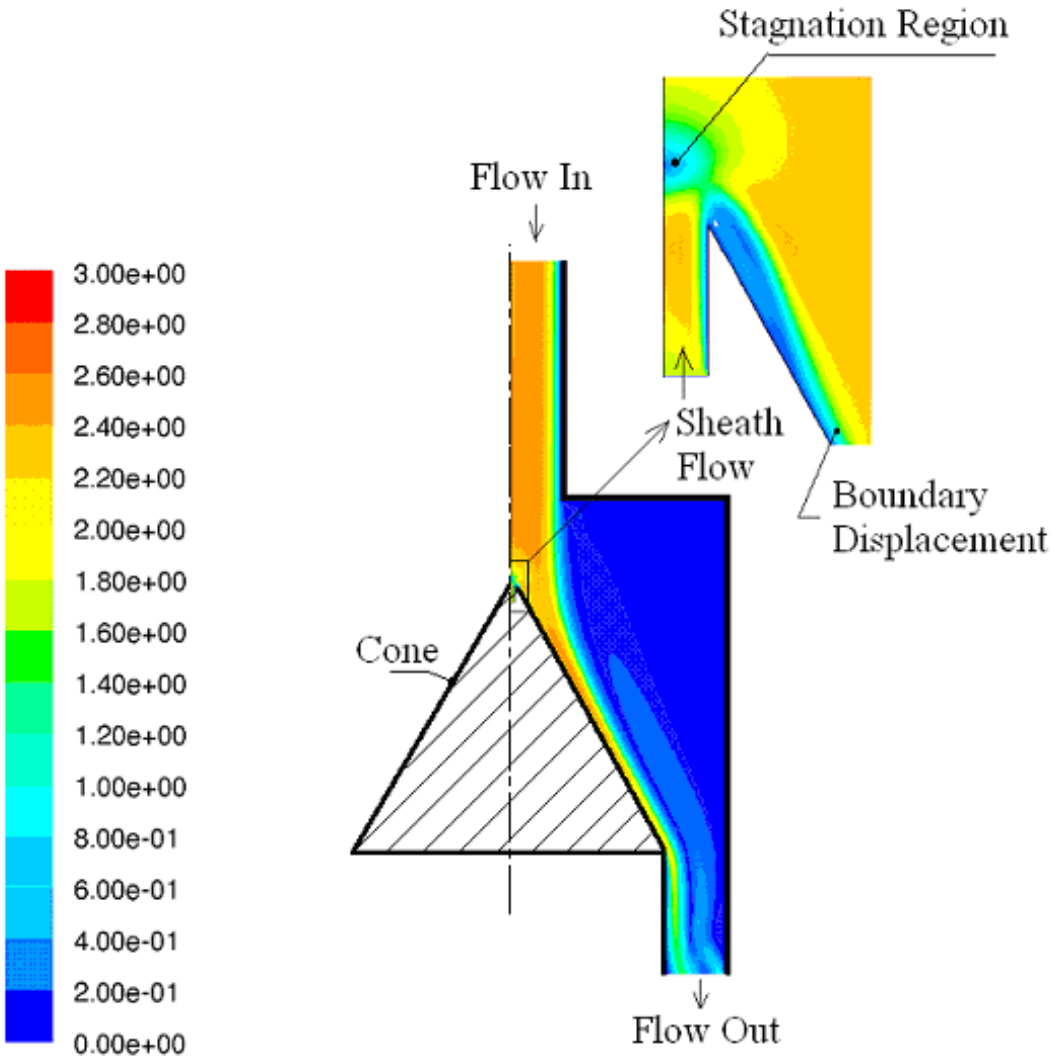

FIG. 5. Numerical analysis showing stagnation region displacement (Hu, 2007).

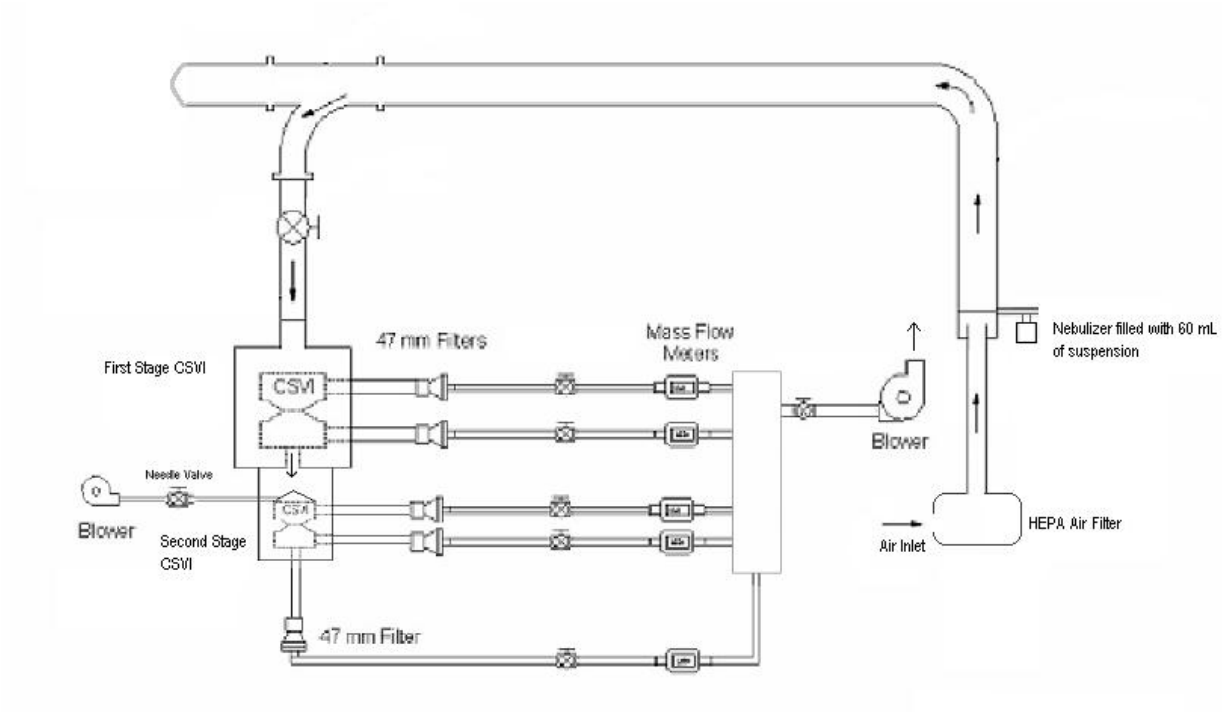

FIG. 6. Setup for testing CSVI with monodispersed polystyrene particles.

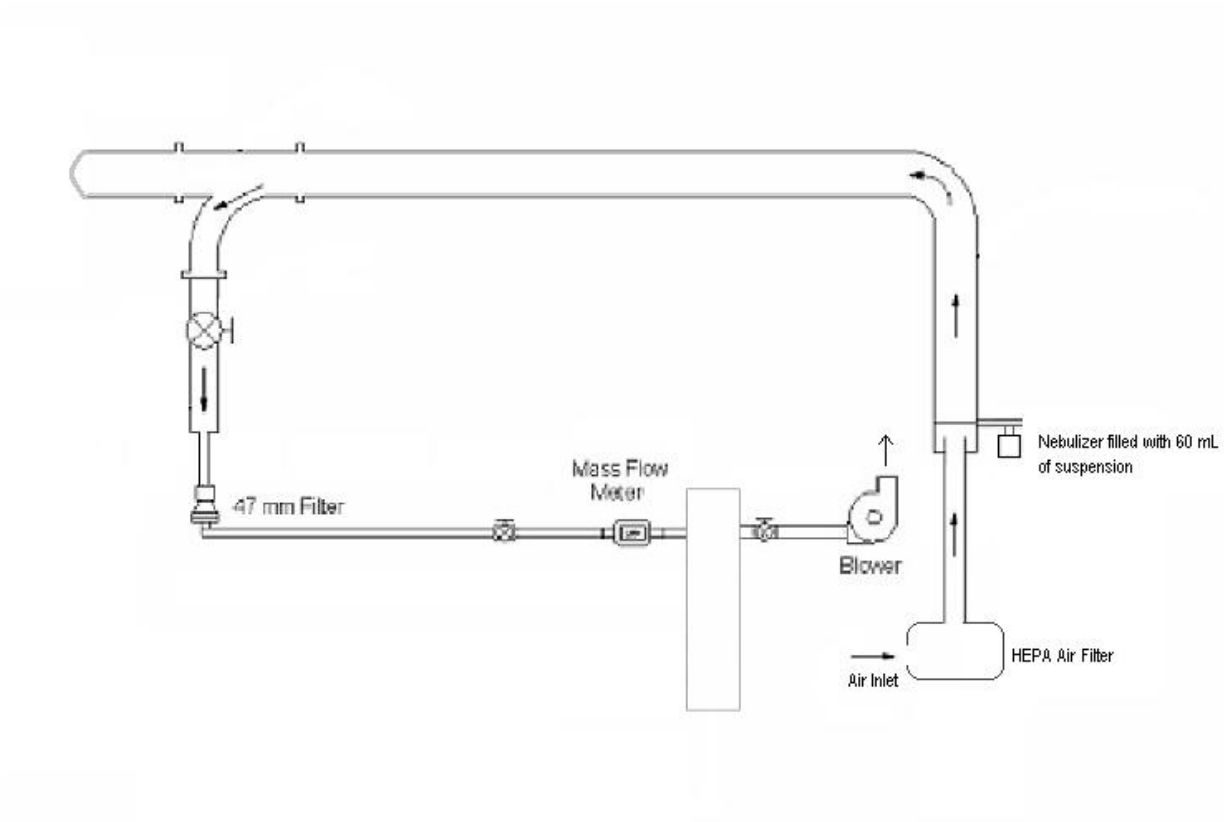

FIG. 7. Setup used for obtaining reference samples of polystyrene aerosol particles.

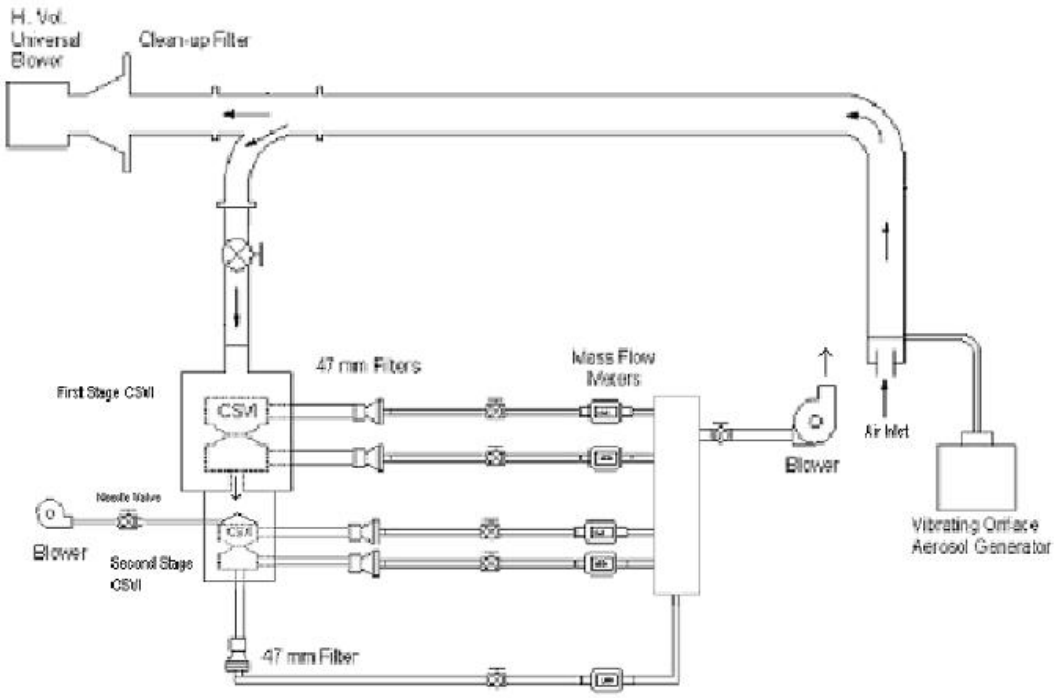

FIG. 8. Setup for testing CSVI with oleic acid aerosol particles.

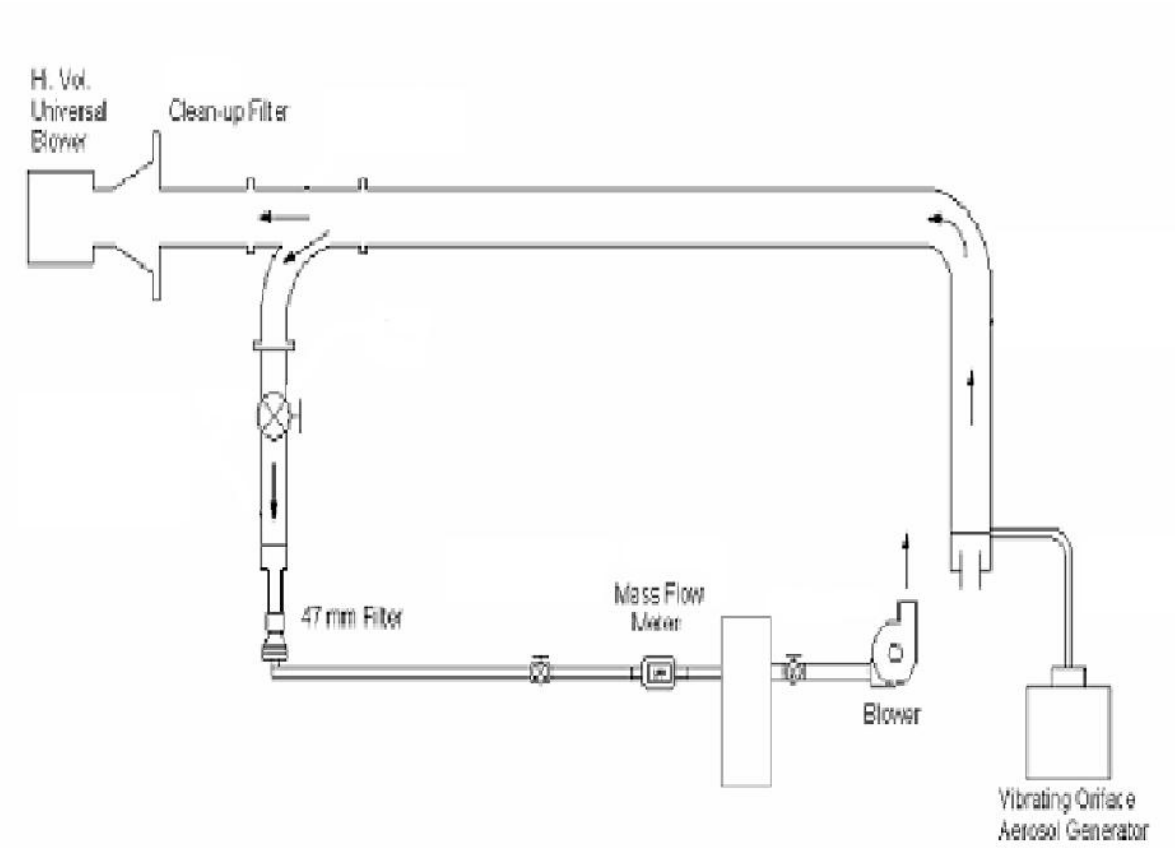

FIG. 9. Setup used for collecting reference samples of oleic acid particles.

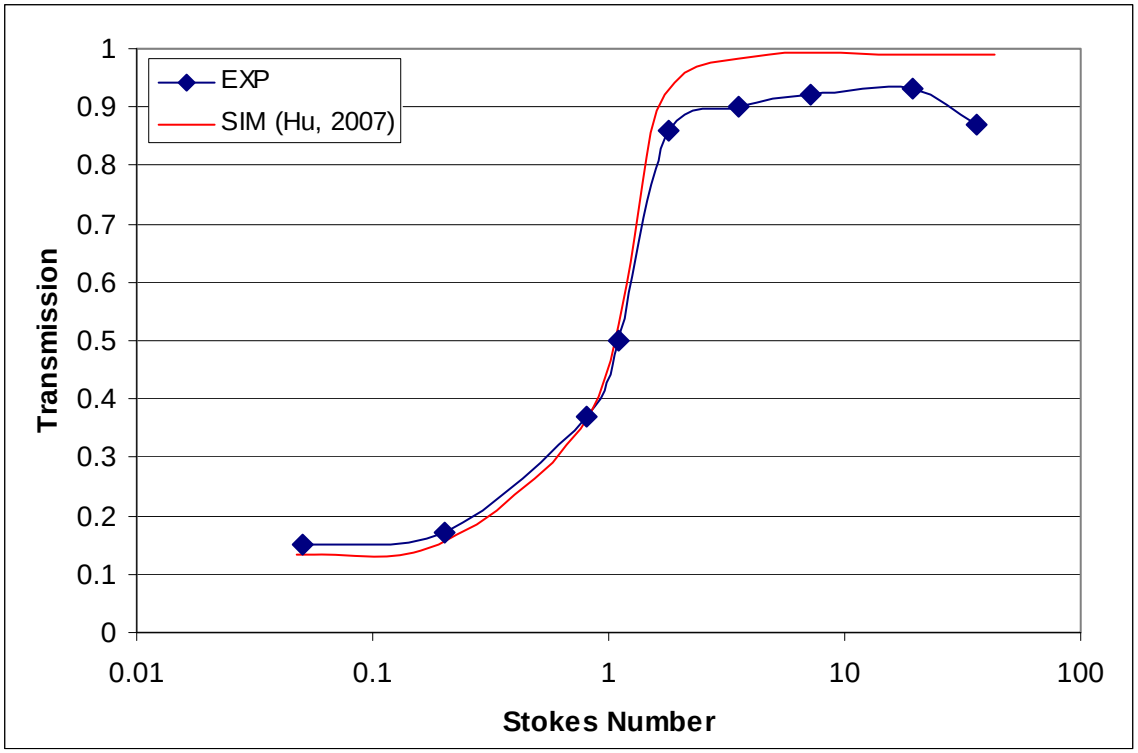

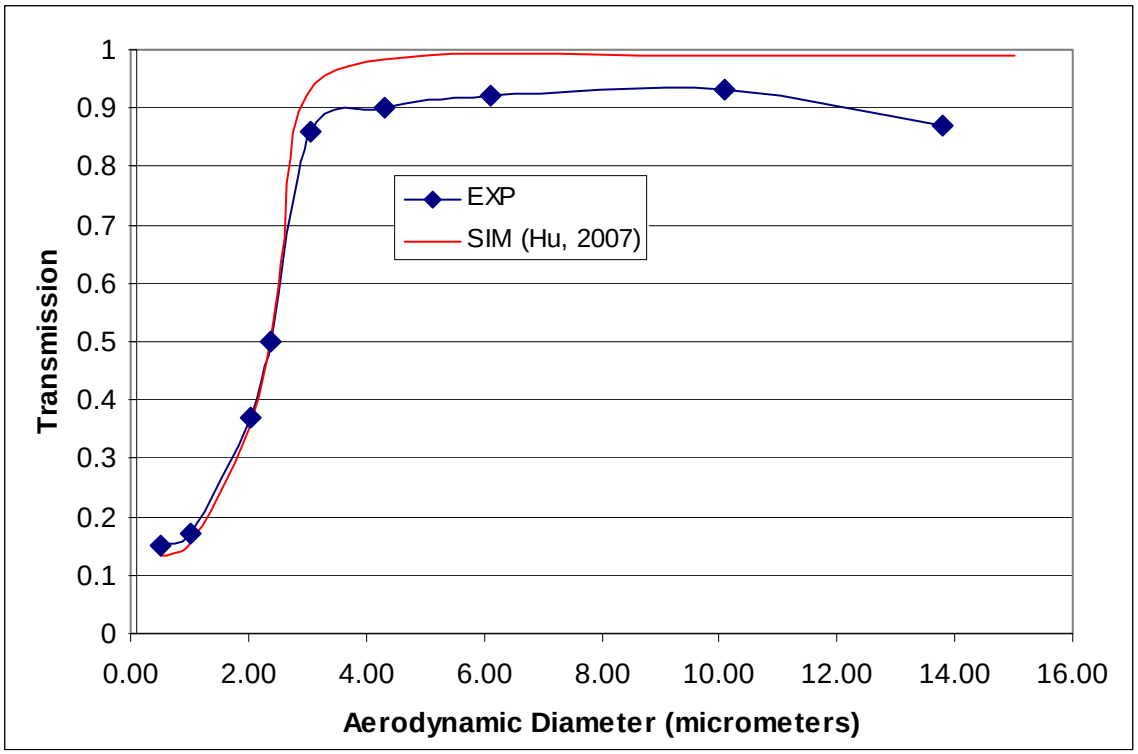

FIG. 10. Transmission curves for the first stage unit operated independently.

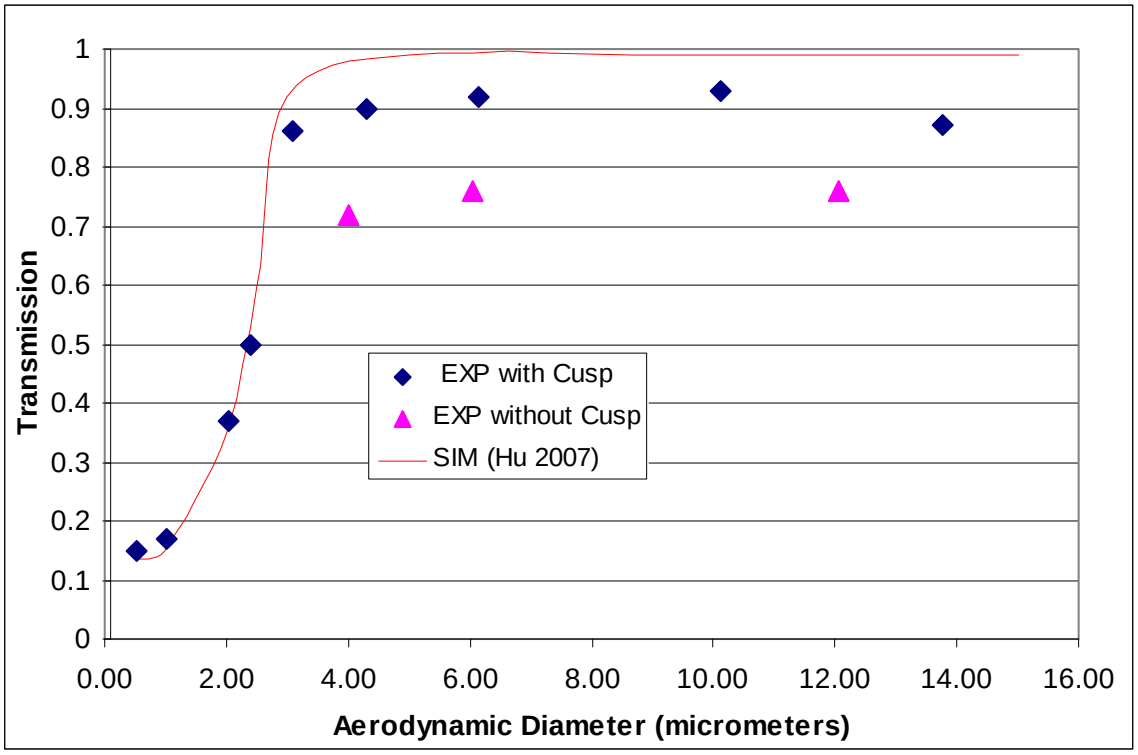

FIG. 11. Transmission curves for the first stage unit operated independently with and without the cusp. The simulation of Hu is for the case of a cusp.

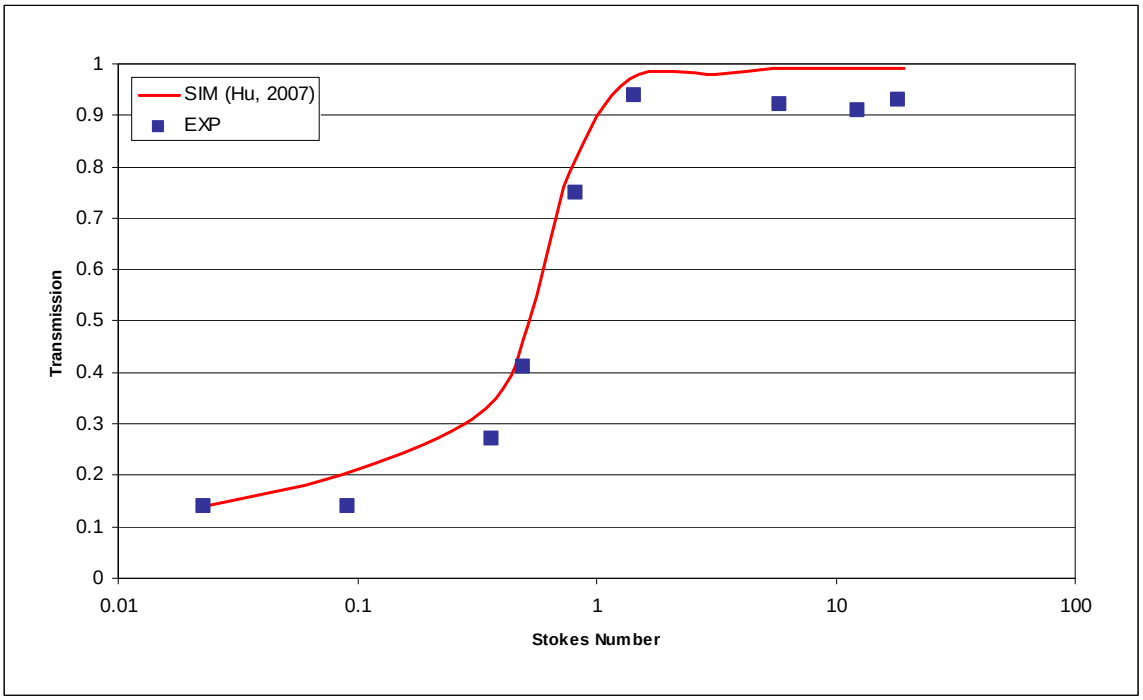

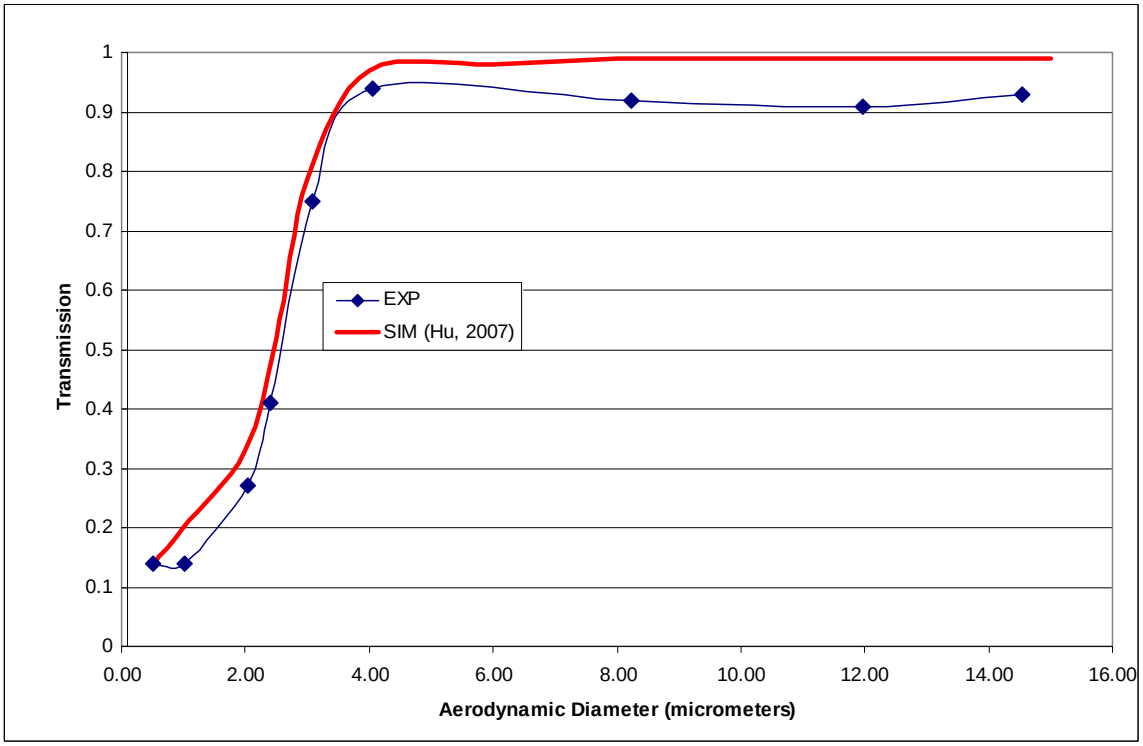

FIG. 12. Transmission curves for the second stage unit operated independently.

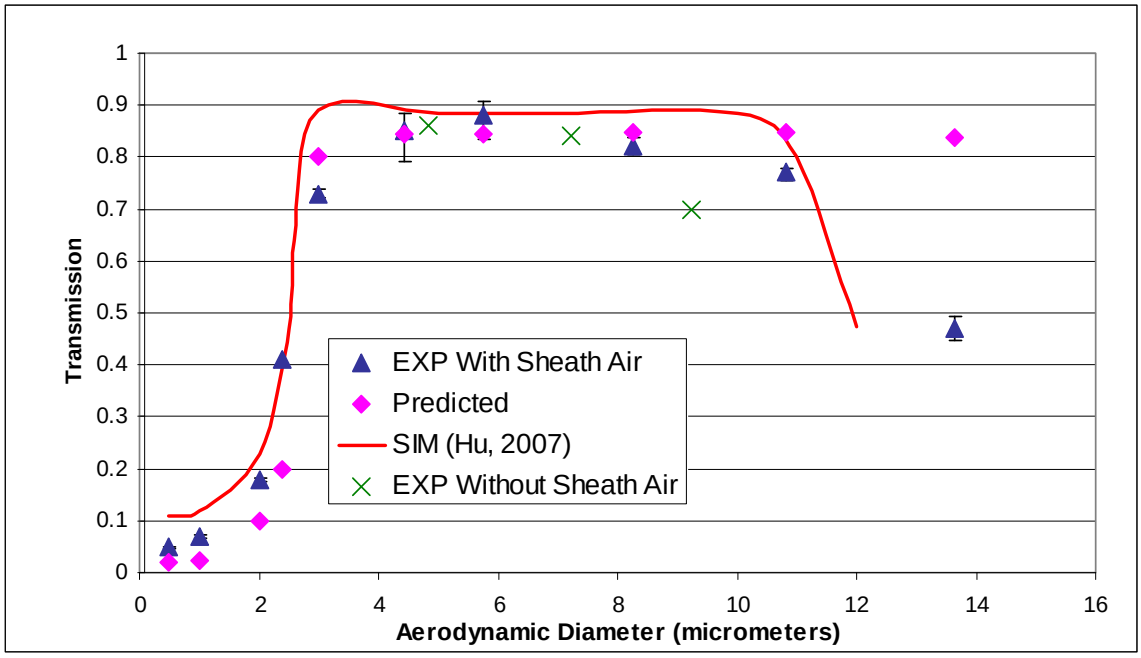

FIG. 13. Actual transmission, numerical simulation, predicted transmission, and transmission for the combined unit as a function of aerodynamic diameter. Simulation results of Hu are for the integrated system with sheath air modeled in 2-D.

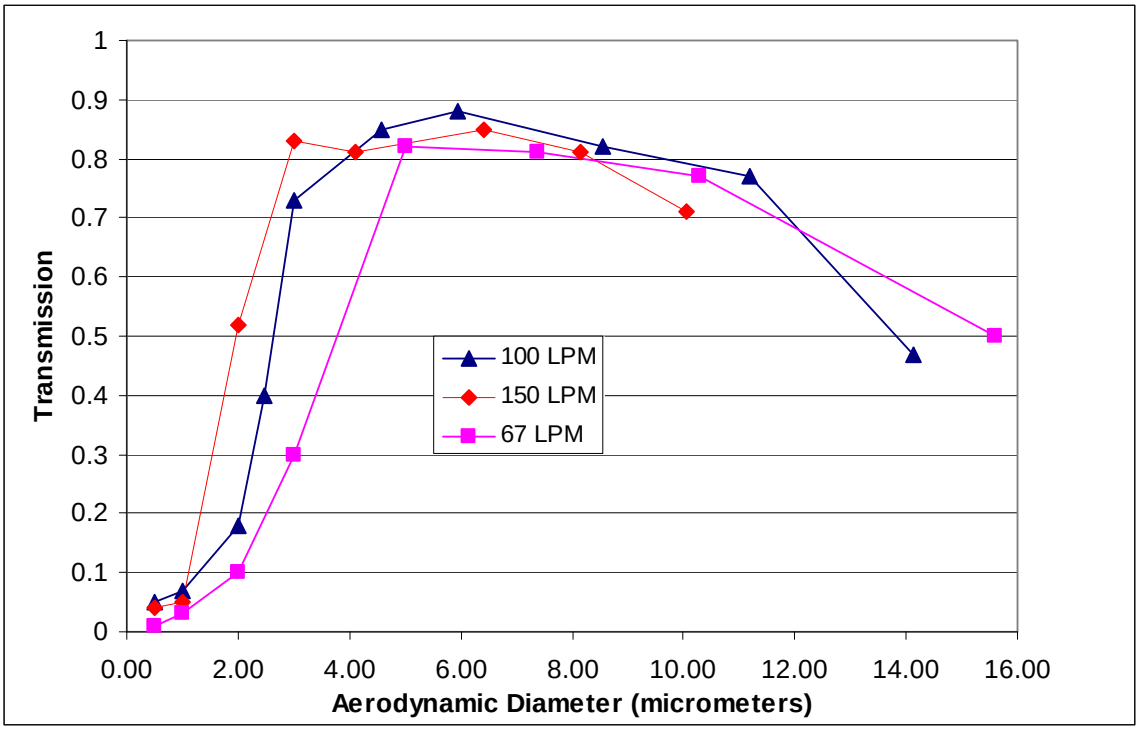

FIG. 14. Transmission of the two-stage integrated unit for flow rates of 100 L/min, 67 L/min and 150 L/min. Sheath air used in all cases.

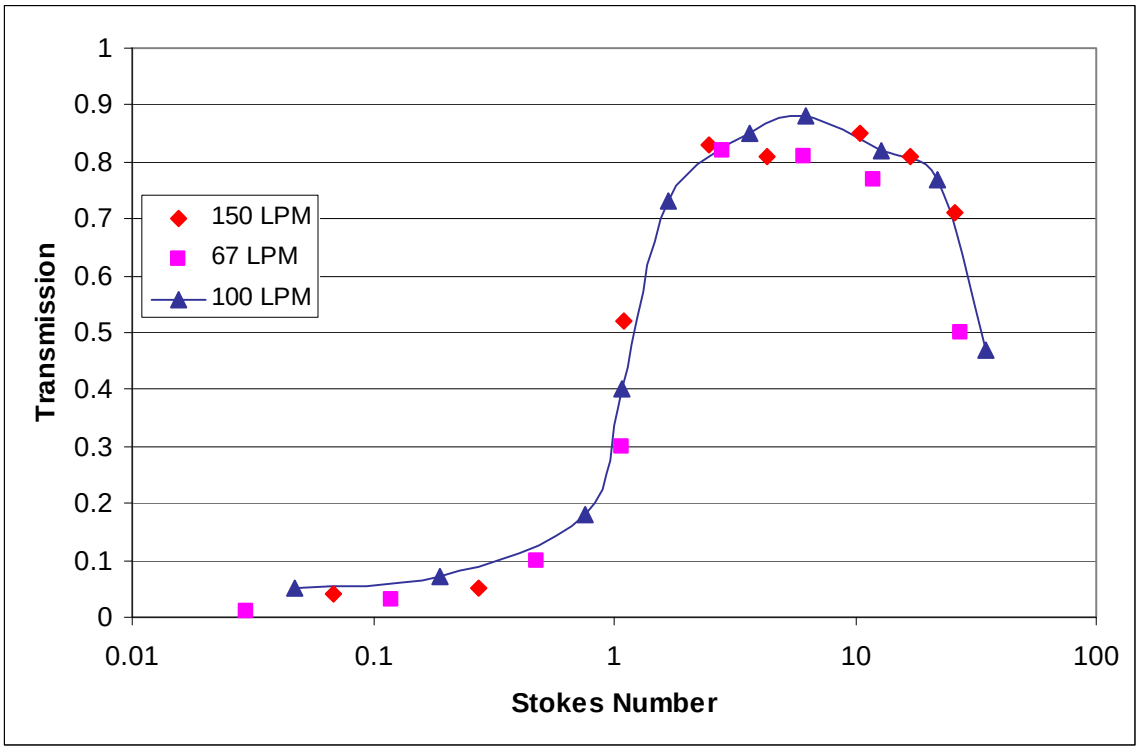

FIG. 15. Transmission of the two-stage unit as a function of the first stage Stokes number. Note that the abscissa would have different values if the scale were based on the second stage Stokes numbers; however, the results do show the overall performance in terms of a Stokes number is relatively independent of flow rate.

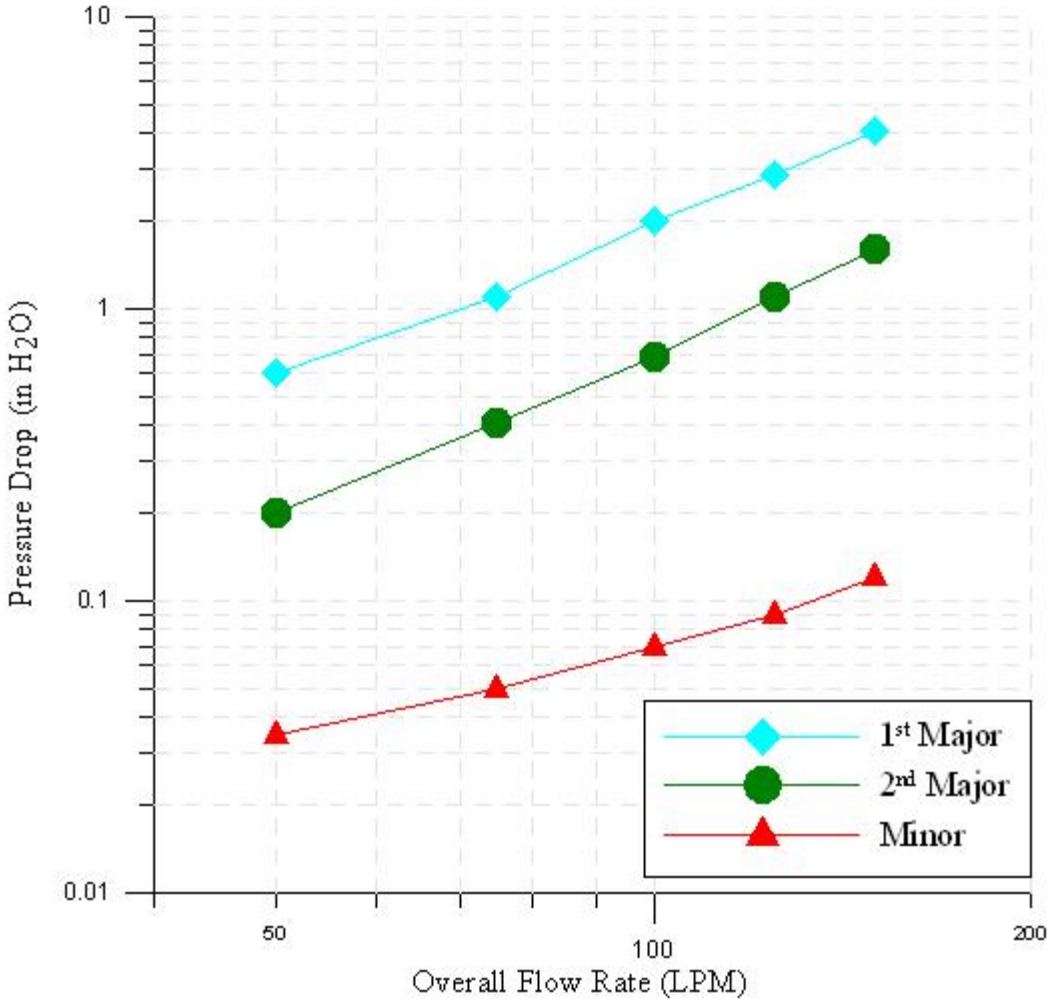

FIG. 16. Pressure drop across each flow tube during operation of the combined system for different flow rates.

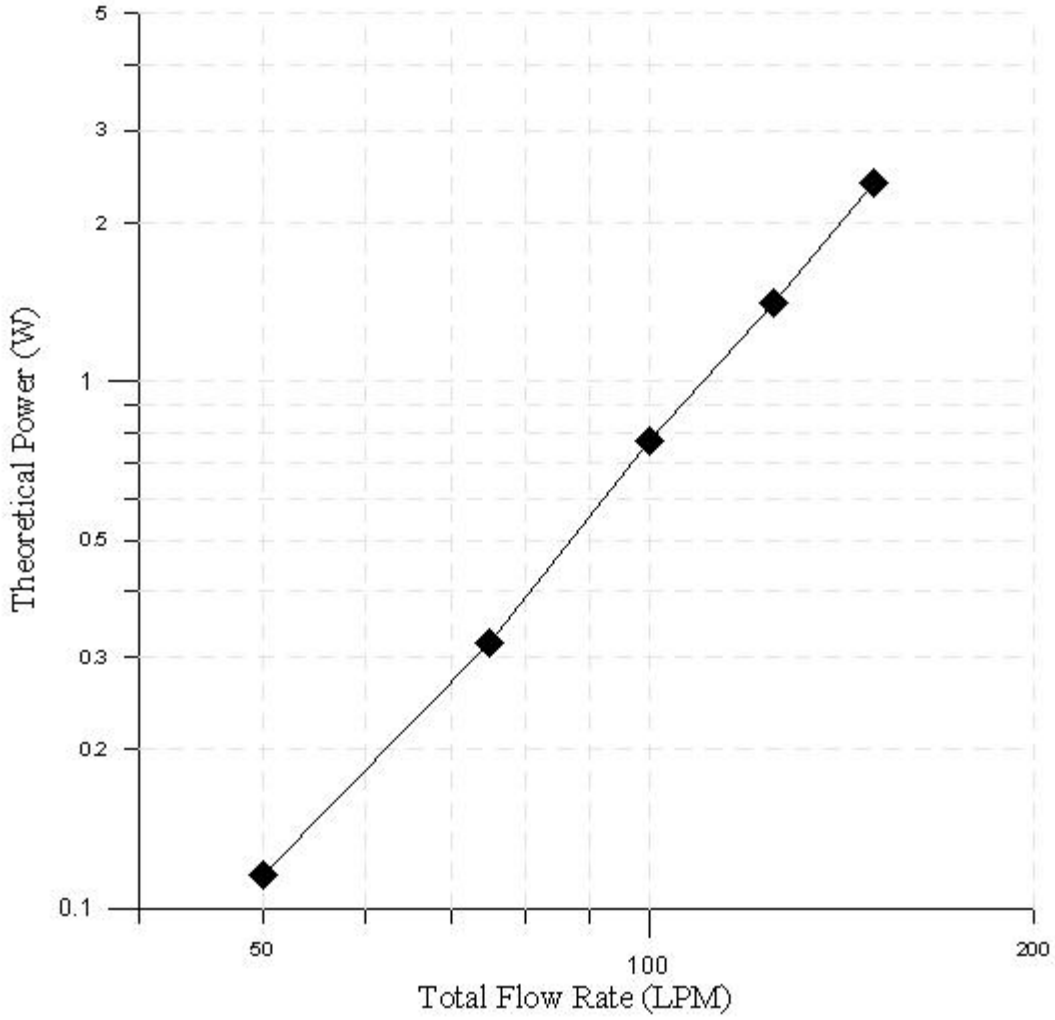

FIG. 17. Ideal power necessary for operation at different flow rates.

APPENDIX C

TABLE A1
Test data for first stage unit operated independently

	Meas. Particle Diam	Test 1	Test 2	Test 3	Ref 1	Ref 2
PSL	0.50	159	145		956	1036
PSL	1.00	285	297		1709	1633
PSL	2.00	388	396	392	1036	1095
Oleic Acid	3.20	522	601		1128	1102
PSL	3.00	770	772	777	897	911
Oleic Acid	5.75	1740	1762	1703	1867	1975
Oleic Acid	8.18	1783	2004	1885	1976	2148
Oleic Acid	13.49	2561	2740	2802	2842	2968
Oleic Acid	18.40	2264	2287		2467	2765
	Without the Cusp					
Oleic Acid	5.36	695	528	583	812	865
Oleic Acid	8.06	405	435	429	564	550
Oleic Acid	16.11	875	902		1124	1204

TABLE A2
Test data for the second stage unit operated independently

	Meas. Particle Diam	Test 1	Test 2	Test 3	Ref 1	Ref 2
PSL	0.50	291	281		2050	2032
PSL	1.00	345	362		2483	2653
PSL	2.00	497	557		1982	1941
Oleic Acid	3.20	490	532	513	1253	1230
PSL	3.00	1564	1540		2064	2100
Oleic Acid	5.43	1474	1491		1592	1557
Oleic Acid	11.00	1860	1505	1648	1811	1817
Oleic Acid	15.99	1400	1330	1150	1400	1440
Oleic Acid	19.40	1456	1495	1468	1537	1624

TABLE A3
Test data for the combined two stage unit

	Meas. Particle Diam	Test 1	Test 2	Test 3	Ref 1	Ref 2
PSL	0.50	4	35		590	630
PSL	1.00	50	40		500	480
PSL	2.00	244	253		900	933
Oleic Acid	2.48	442	395	420	1128	1102
PSL	3.00	1564	1540		2064	2173
Oleic Acid	5.90	1200	1330	1342	1416	1632
Oleic Acid	7.68	2440	2630	2593	2725	3055
Oleic Acid	11.03	1560	1605	1629	2039	1847
Oleic Acid	14.45	2094	2041	2104	2661	2731
Oleic Acid	18.21	1385	1240	1360	2661	2737
	No Sheath Air					
Oleic Acid	6.86	3000	3072		3500	3590
Oleic Acid	9.64	1200	1300	1342	1416	1632
Oleic Acid	12.31	1472	1528	1540	2179	2182

TABLE A4
Test data for the combined unit operated at 150 L/min and 67 L/min

	150 L/min Meas. Particle Diam	Test 1	Test 2	Test 3	Ref 1	Ref 2
PSL	0.5	36	45		762	771
PSL	1	43	33		796	833
PSL	2	502	510		866	1080
PSL	3	1372	1745		1881	1855
Oleic Acid	5.31	1372	1745	1552	1935	1954
Oleic Acid	8.26	1323	1467	1494	1649	1718
Oleic Acid	10.51	1888	1935	1986	2379	2390
Oleic Acid	12.98	2020	1585	1907	2670	2746

	67 L/MIN Meas. Particle Diam	Test 1	Test 2	Test 3	Ref 1	Ref 2
PSL	0.5	2	14		1054	1065
PSL	1	20	56		1269	1273
PSL	2	152	155		1486	1478
PSL	3	610	588		1954	1989
Oleic Acid	5.96	1660	1423	1566	1816	1961
Oleic Acid	9.53	1944	1826	1867	2320	2340
Oleic Acid	13.28	1945	1862	1930	2550	2510
Oleic Acid	19.68	1022	1074	1187	2187	2498

TABLE A5
Data for pressure drop readings and power calculations
Ideal Power Consumption- Work

	L/MIN	M^3/s	dP (in H20)	dP (Pa or N/m^2)		
Total Flow Rate	100	0.001667				
1st Major Flow Rate	90	0.0015	2	498	0.747	
2nd	9	0.00015	0.68	169.32	0.025398	
Minor	1	1.67E-05	0.07	17.43	0.0002905	
			2.75	total	0.7726885	watts

	L/MIN	M^3/s	dP (in H20)	dP (Pa or N/m^2)		
Total Flow Rate	50	0.000833				
1st Major Flow Rate	45	0.00075	0.6	149.4	0.11205	
2nd	4.5	0.000075	0.2	49.8	0.003735	
Minor	0.5	8.33E-06	0.035	8.715	7.263E-05	
				total	0.1158576	watts

	L/MIN	M^3/s	dP (in H20)	dP (Pa or N/m^2)		
Total Flow Rate	150	0.0025				
1st Major Flow Rate	135	0.00225	4.1	1020.9	2.297025	
2nd	13.5	0.000225	1.6	398.4	0.08964	
Minor	1.5	0.000025	0.12	29.88	0.000747	
				total	2.387412	watts

	L/MIN	M^3/s	dP (in H20)	dP (Pa or N/m^2)		
Total Flow Rate	75	0.00125				
1st Major Flow Rate	67.5	0.001125	1.1	273.9	0.3081375	
2nd	6.75	0.000113	0.41	102.09	0.0114851	
Minor	0.75	1.25E-05	0.05	12.45	0.0001556	
				total	0.3197783	watts

	L/MIN	M^3/s	dP (in H20)	dP (Pa or N/m^2)		
Total Flow Rate	125	0.002083				
1st Major Flow Rate	112.5	0.001875	2.9	722.1	1.3539375	
2nd	11.25	0.000188	1.1	273.9	0.0513563	
Minor	1.25	2.08E-05	0.09	22.41	0.0004669	
				total	1.4057606	watts

VITA

Name: Daniel Edward LaCroix

Address: Aerosol Technology Lab
Department of Mechanical Engineering
Texas A&M University, College Station, TX 77843-3123

Education: B.S. Engineering Science, Trinity University, San Antonio, TX

M.S., Mechanical Engineering, Texas A&M University, College Station, TX

Email: dlacroix21@gmail.com